The biomechanics of foraging determines face length among kangaroos and their relatives

D. Rex Mitchell, Emma Sherratt, Justin A. Ledogar & Stephen Wroe

SUPPLEMENTARY MATERIAL

Geometric morphometrics

Sixteen species of macropods were sampled for 3D coordinate data. The dataset included 236 intact crania from the Australian Museum, the Queensland Museum, and the Natural History Museum of the University of New England. Adult specimens were prioritised; identified on the basis of eruption of the fourth molar [1]. Landmarks were digitised on the crania using a G2X Microscribe (Immersion Corporation, San Jose, CA) by one researcher (DRM). Thirty-two landmarks were digitised at homologous locations on the cranium, including teeth, foramina, and suture junctions (Fig. S1, Table S1). The landmarks used were based on those of a previous macropod study [2], with four exceptions: (1) Paired landmarks 1 and 22 of the original study, the fronto-parietal suture at the intersection of the temporal crest, were changed to where the fronto-parietal suture meets the dorsal rim of the orbit. The original landmark location was found to have high intraspecific variation, with medial expansion of the temporal fossa found in older individuals [3]; (2) Paired landmarks 9 and 29 [2], the latero-posterior-most point of the last functional molar, were removed after initial analysis because the location of the M4 displayed a great deal of variation between adults of different ages due to the nature of molar progression [4] and the influence of age was not relevant to the main questions of this study; (3) Landmark 17 [2], Bregma, was excluded because it was not visible for many specimens that had complete medial convergence of the temporal fossae; (4) Landmark 21 [2], the inter-

premaxillary suture at the alveolar margin, was removed as this point was often eroded away in weathered specimens.

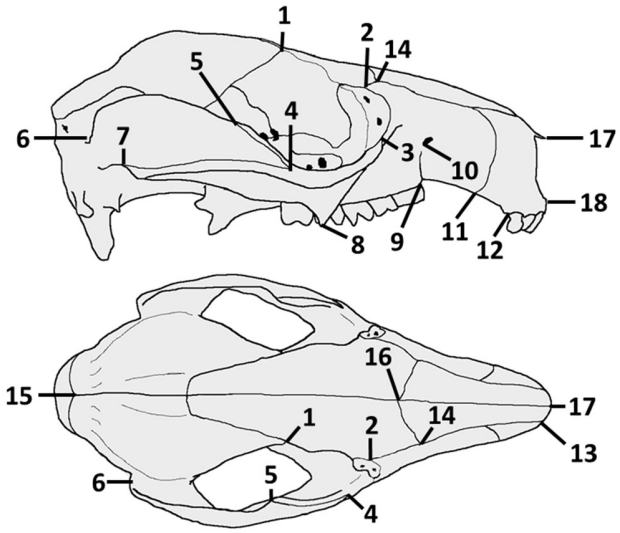

Figure S1: Landmark locations on a macropod cranium. Landmarks 19-32 on the left side are paired with landmarks 1-14 on the right side.

Table S1: Landmarks used for morphometric analyses

Number	Location of Landmarks
1 and 19	Fronto-parietal suture at the lateral frontal ridge
2 and 20	Fronto-maxillary-lacrimal junction
3 and 21	Zyomatico-maxillary-lacrimal junction
4 and 22	Anterior-most point of the zygomatic process on the temporal bone
5 and 23	Dorsal-most point of the zygomatico-temporal suture on the dorsal edge of the zygomatic arch
6 and 24	Superior root of the zygoma on the temporal bone
7 and 25	Posterior end of the zygomatico-temporal suture
8 and 26	Ventral-most point of the anterior end of the zygomatic arch Masseteric process
9 and 27	Alveolar margin at the latero-anterior-most point of the first premolar
10 and 28	Infraorbital foramen

11 and 29	Maxillary-premaxillary suture at the alveolar margin
12 and 30	Alveolar margin at the posterior-most point of the 3rd incisor
13 and 31	Naso-premaxillary suture at the margin of the nasal aperture
14 and 32	Fronto-naso-maxillary junction
15	Lambda
16	Naso-frontal suture at the midline
17	Tip of the nasal bone at the midline
18	Interpremaxillary suture at the ventral margin of the nasal aperture

Diet groups

Each species was categorised by diet (Table S2). The dominant vegetation type of each species within its natural environment was prioritised [5]. These preferences amounted to six categories: roots and tubers, fungi, fruit, a mixed diet, browse, and graze [6]. Diet allocations were most often via consensus of the literature [7], but there were some exceptions:

(1) The rufous bettong (*Aepyprymnus rufescens*) has not previously been allocated a dietary category in the literature. This species has an omnivorous diet that includes invertebrates, tuberous roots, grass leaves and seeds, perennial herbs, flower buds, fruit, fungi and gum exudate [8-9]. Most research indicates that the diet of *A. rufescens* is dominated by the roots and tubers of native and introduced plants [8-12]. However, dietary composition is subject to seasonal availability and diet can include up to 80% graze [13] (however this value was derived from carbon isotopes and may still represent the roots of grasses). Given that the literature is dominated by claims of a rhizophagous diet, this species was classed as a specialist of fibrous roots and tubers.

(2) The musky rat-kangaroo (*Hypsiprymnodon moschatus*) is omnivorous, with a diet that includes fruit, fungi, seeds and insects. Most research indicates that the diet is dominated by fruits and supplemented with fungi and invertebrates [9,14-15]. This species was classed as a fruit specialist for accuracy, although previously classed as a fungivore [7].

(3) The rufous hare-wallaby, or mala (*Lagorchestes hirsutus*), incorporates a wide range of items into its diet, including seeds, leaves, forbs and fruits. There is a preference for softer, less fibrous foods such as fruits and seeds in more productive months; while monocot and dicot leaves are more frequently eaten in drier months [16]. Thus, although this species is sometimes described as a browser [17] or seed specialist [18], it was classed as a mixed feeder (intermediate browser/grazer) for the purposes of this study [6].

(4) The red-necked wallaby (*Macropus rufogriseus*) can include a large proportion of browse in its diet where native grasses are rare or very limited, such as high alpine environments [19] or exotic environments upon its introduction [20]. However, such cases of extreme diet shift have also been observed for other grazing species when their preferred foods are scarce [21]. This species prefers a habitat comprised of sclerophyllous forestation [22] and in such habitats they preferentially select native grasses, resulting in a diet of up to 84% graze, and incorporate forbs only as a secondary food source [11,23]. Therefore, *M. rufogriseus* is classed it as a grazer, in terms of its general preference within its natural environment.

Table S2: List of species, number of specimens and allocated diets

Species	Specimens	Diet
Aepyprymnus rufescens	15	Roots
Bettongia penicillata	16	Fungi
Dendrolagus dorianus	19	Browse
Dendrolagus lumholtzi	16	Browse
Hypsiprymnodon moschatus	7	Fruit
Lagorchestes hirsutus	13	Mixed
Macropus dorsalis	10	Graze
Macropus giganteus	15	Graze
Macropus robustus	15	Graze
Macropus rufogriseus	15	Graze
Macropus rufus	15	Graze
Onychogalea fraenata	14	Mixed
Petrogale penicillata	15	Mixed
Potorous tridactylus	15	Fungi
Thylogale stigmatica	21	Mixed
Wallabia bicolor	15	Mixed

Morphometric analyses

All analyses were conducted in in R v.3.2.5 [24]. Firstly, to account for measurement error, one specimen per species was digitised twice by the same researcher. Mean Procrustes distances between specimens and between the two replicates were calculated. The proportion of variation found between specimens was calculated as a percentage of the combined variation contributed from between the replicates and between the specimens [25]. The measurement error was considered negligible if it contributed 5% or less of this variation. We found that 4.62% of the total variation was due to inconsistencies in digitisation; indicating that the results are more than 95% repeatable.

Most specimens examined did not offer clear indications of sex and so sexual dimorphism was not explored in this study. Previous morphometric analyses have all found

little statistical support for sexual dimorphism in cranial features of macropods, with exception to *M. rufus* [2,26]. In such cases, variation between species was greater than variation attributed to sexual dimorphism [2,26]. Given the broad taxonomic nature of this study, pooling of sexes for morphometric analyses was considered reasonable.

The data were subjected to a generalised Procrustes superimposition to remove non-shape variation [27], using the 'gpagen' function in the Geomorph R package (v. 3.0.2) [28]. As most landmarks were paired, the shape variables for the symmetric component of shape were extracted [29] using the 'bilat.symmetry' function (Geomorph). We assessed evolutionary allometry and diet, while accounting for phylogenetic relationships, by conducting a phylogenetic regression on shape data [30], using the 'procD.pgls' function (Geomorph). The phylogenetic tree (Fig. S2) was generated using Mesquite v. 3.2 [31] using time-calibrated molecular data [32-33].

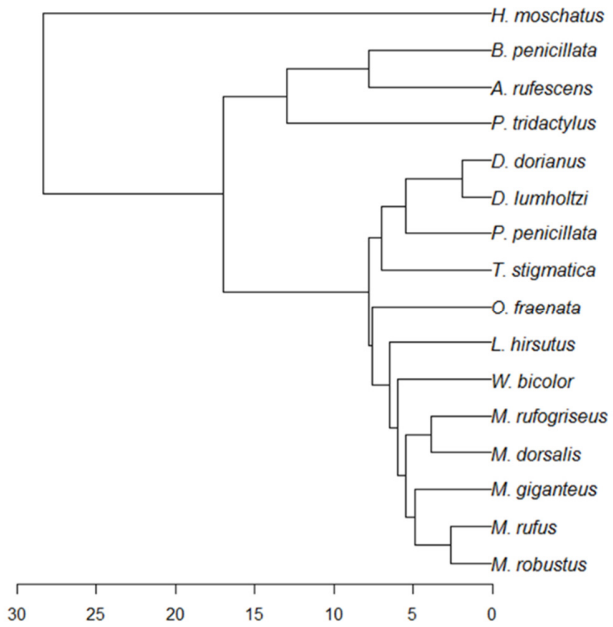

Figure S2: Phylogenetic tree of Macropodiformes. Scale = million years

Principal component analysis of the coordinate data (PCA) was then performed to examine shape variation and distributions of each species in a shape (tangent) space. PC axes were explained in relation to morphology by performing correlations on PC scores and ratios (indices) generated from linear measurements between landmarks of interest, obtained with the 'interlmkdist' function (Geomorph). To visualise the shape variation associated with the main PC axes, we used a 3D warping approach [34]. A surface mesh (triangular isosurface) of a morphologically average specimen (*T. stigmatica*), was created in Mimics (version 17) by thresholding the tomograph for bone, generated by X-ray computed tomography (CT). The average mesh was then warped using thin-plate spline (TPS) approach to represent the average shape in the data. The mesh was then warped to the shapes representing the minima and maxima of each respective PC axis using TPS for a visual interpretation of the principal components.

Since the muzzle morphology is a functionally relevant trait, we calculated its relative length from the landmark data (muzzle tip to naso-frontal suture/muzzle tip to lambda), then conducted a separate generalised least squares model using the 'gls' function from the nlme R package [35]. We tested two separate models: muzzle length ~ diet, and muzzle length ~ log(centroid size) + diet.

Finite element analysis

A morphologically average specimen of each species, in good condition for CT scanning and modelling, was selected from the shape analysis. Smaller specimens were scanned at either the University of New South Wales, on a Inveon microCT (Siemens, Victoria), or the University

of New England, on a Phoenix v-tome-x Industrial High-Resolution CT scanner (GE Sensing & Inspection Technologies; Wunstorf, Germany), with slice widths ranging from 0.6-1.0mm at up to 300ms exposure. Larger species were carried out on a Siemens somatom definition AS CT scanner; slice width 0.75 with 0.70 increments.

Model assembly

Construction of FEMs largely follow a combination of protocols used Wroe, et al. [36] and Ledogar, et al. [37]. Surface meshes were generated using Mimics v. 18.0, converted to solid (i.e., volumetric) FEMs using 3-Matic Research v.10.0, and imported into Strand7 v.2.4.4 finite element software. The FEMs were composed of approximately 1.7 million 3D four-noded tetrahedral elements. Models were assigned homogeneous and isotropic material properties, a method considered appropriate for comparative studies that aim to identify the influence of shape, rather than predict absolute stress/strain values [38-41]. Average material property values for mammalian bone were allocated to the models (Young's modulus: E = 20 GPa; Poisson's ratio: v = 0.3) [42-43]. Despite previous analyses identifying that homogeneous material properties influence absolute strain magnitudes, they have little effect on relative strain distributions, and thus are acceptable for comparative contexts [44]. The results from this methodology therefore represent relative, rather than absolute predictions and should be interpreted as parameters estimated from cranial geometry alone, that do not reflect actual in vivo bite forces or resulting strain [45].

Muscle Forces and loading conditions

Seven masticatory muscle divisions, described for macropods [46], were individually allocated to each model: the deep masseter (MD), intermediate masseter (MI), superficial masseter (MS), zygomaticomandibularis (Z), lateral pterygoid (PL), medial pterygoid (PM), and temporalis (T) muscles. The maximum cross-sectional area (CSA) of each muscle was obtained from a dissection of a red-necked wallaby (*Macropus rufogriseus*), from photographs of each removed muscle using ImageJ (v. 1.50i). The muscle proportions obtained were comparable to previous results from other macropod species [43,46] and are presented in Table S3.

Table S3: Muscle proportions from *M. rufogriseus* dissection

Muscle	CSA (cm^2)	Proportion
MD	1.478	0.101
MI	2.315	0.158
MS	2.150	0.147
Z	1.586	0.108
M(total)	7.529	0.514
T	3.901	0.266
PL	1.641	0.112
PM	1.573	0.107
P(total)	3.214	0.219

As 300 kilo-Newtons are produced for every square metre of striated muscle [47], magnitudes of muscle force were estimated by multiplying the CSA by a constant value for muscle stress of 0.3 $N.mm^{-2}$. Muscle forces were then scaled, from the *M. rufogriseus* specimen, to each other species using a 2/3 power rule based on cranial volume [39,48] (Table S4).

Table S4: Scaled muscle forces for all FEMs

	Mass	MD	MI	MS	Z	PL	PM	T	Total
A. rufescens	2.197	21.99	34.44	31.98	23.59	24.41	23.40	58.03	217.85
B. penicillata	1.003	13.99	21.91	20.35	15.01	15.53	14.89	36.92	138.60
D. dorianus	7.621	43.28	67.80	62.96	46.45	48.06	46.07	114.24	428.85
D. lumholtzi	4.225	35.53	55.65	51.68	38.12	39.45	37.81	93.77	352.00
H. moschatus	0.754	10.10	15.82	14.69	10.84	11.22	10.75	26.66	100.09
L. hirsutus	1.771	17.01	26.65	24.75	18.26	18.89	18.11	44.90	168.56
M. dorsalis	10.639	36.02	56.42	52.40	38.65	39.99	38.34	95.07	356.90
M. giganteus	44.681	89.38	140.00	130.02	95.91	99.24	95.12	235.91	885.57
M. robustus	26.668	74.93	117.37	109.00	80.41	83.20	79.75	197.77	742.42
M. rufogriseus	18.957	62.63	98.10	91.11	67.21	69.54	66.66	165.31	620.56
M. rufus	39.392	101.91	159.63	148.25	109.36	113.15	108.46	268.99	1009.76
O. fraenata	2.511	22.58	35.37	32.85	24.23	25.07	24.03	59.60	223.73
P. penicillata	6.999	33.46	52.41	48.67	35.90	37.15	35.61	88.31	331.51
P. tridactylus	1.661	14.89	23.32	21.66	15.98	16.53	15.85	39.30	147.54
T. stigmatica	6.122	30.15	47.23	43.86	32.36	33.48	32.09	79.59	298.77
W. bicolor	10.771	48.66	76.22	70.79	52.22	54.03	51.79	128.43	482.13

Crania and dentaries were arranged with a gape angle of 10-10.5^{o} at the incisors using Geomagic Studio 2014. To apply muscle forces to the models, groups of plate elements representing each muscle origin were created. Muscle forces were applied to these plates using Boneload, with muscle force vectors oriented toward their respective insertion sites on the mandible. This method accounts for muscle fibres wrapping around curved surfaces of bone [49]. Loaded plates were then imported into the FEMs, modeled as 3D membranes (thickness = 0.0001mm), and “zipped” at their nodes to the surface faces of elements.

To simulate a bilateral incisor bite, a single node was chosen at both temporomandibular (TMJ) joints and constrained against translation in all directions, while an individual node was also chosen on the tip of each first incisor and constrained in the dorso-ventral axis only. These constraints create an axis of rotation around the TMJs upon the application of muscle forces, inducing deformation in the craniofacial skeleton and generating reaction forces at the constrained nodes [37].

Mechanical efficiency

The body mass (BM) was estimated for each specimen, using a formula for diprotodont marsupials derived from cranio-mandibular linear measurements [50]. After solving the models, bite reaction force (BRF) was obtained for each loading from the restrained nodes at the incisors. The correlation between logBM and logBRF was plotted across species (Fig. S3).

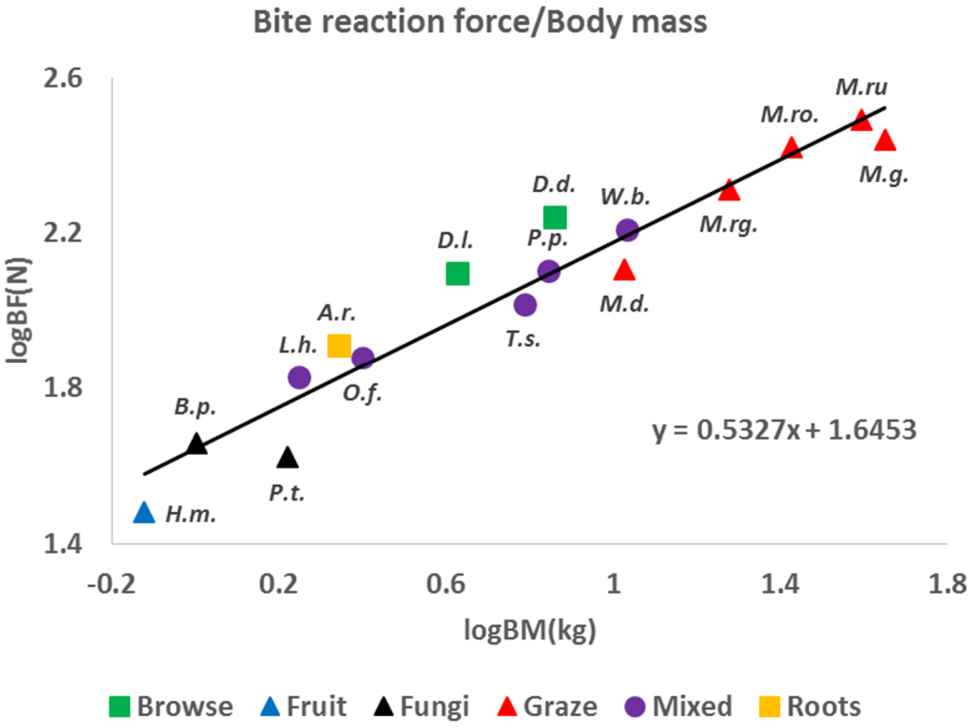

Figure S3: Regression of bite reaction force and body mass across all species.

The regression line represents the expected BRF for a given size across all species examined. A mechanical efficiency quotient (MEQ) was generated from the residuals of the

regression for each species in order to compare the mechanical efficiency across species of different body mass.

$$MEQ = \mathbf{100} + 100 * (residual_i)$$

Where **100** is the arbitrary value given to the regression line, and $residual_i$ is the observed BRF_i minus the predicted value of BRF_i obtained from the regression line. This is similar to the bite force quotient [51], and is based on the difference between an actual bite reaction force obtained from the models and bite reaction force that would be 'average' for a macropodiform of a given body mass. The MEQ thus offers an indication of mechanical efficiency, derived from the disparity between expected BRF for a given BM (MEQ = 100), versus the observed value, represented by an increase (MEQ >100) or a decrease (MEQ <100). We then used a linear model to test for a correlation between muzzle length and MEQ values.

After assessing biomechanical advantage, we wished to examine performance. However, the strain magnitudes from the initial FEMs were highly influenced by the variation contributed by the range of muzzle lengths and resulting mechanical advantage across species. Since bite force diminishes with increased distance from the temporomandibular joint [52], all species were performing different biting actions for their size in the initial scaled models. The species with the longest muzzles gave the lowest BRF values and, therefore, lowest strain values, while species with short muzzles displayed higher BRF and, therefore, higher relative strain magnitudes. To compare performance more meaningfully, we aimed to standardise this variation and ensure that all species were performing an equivalent bite, relative to body mass. To achieve this, muscle forces were adjusted for each model such that they generated the 'average' or expected BRF for a macropodiform of that body mass [53] as identified by the

regression line in Figure S3. This removed the variation attributed to mechanical efficiency. Adjusted muscle forces are shown in Table S5.

Table S5: Muscle forces adjusted to predicted bite force

	MD	MI	MS	Z	PL	PM	T	Total
A. rufescens	18.10	28.36	26.33	19.43	20.10	19.27	47.78	179.37
B. penicillata	13.60	21.30	19.78	14.59	15.10	14.47	35.90	134.75
D. dorianus	31.38	49.16	45.65	33.68	34.84	33.40	82.83	310.94
D. lumholtzi	27.02	42.33	39.31	29.00	30.00	28.76	71.33	267.75
H. moschatus	12.69	19.88	18.46	13.62	14.09	13.51	33.50	125.77
L. hirsutus	15.18	23.78	22.08	16.29	16.85	16.15	40.06	150.39
M. dorsalis	43.73	68.50	63.62	46.93	48.56	46.54	115.43	433.31
M. giganteus	107.88	168.98	156.94	115.77	119.78	114.82	284.75	1068.92
M. robustus	72.00	112.77	104.73	77.26	79.94	76.63	190.03	713.36
M. rufogriseus	64.37	100.82	93.64	69.07	71.47	68.51	169.90	637.78
M. rufus	102.62	160.73	149.27	110.12	113.93	109.21	270.85	1016.74
O. fraenata	21.55	33.75	31.35	23.12	23.93	22.93	56.88	213.51
P. penicillata	32.83	51.42	47.76	35.23	36.45	34.94	86.66	325.30
P. tridactylus	20.52	32.14	29.85	22.02	22.79	21.84	54.17	203.34
T. stigmatica	33.49	52.46	48.72	35.94	37.19	35.65	88.40	331.86
W. bicolor	46.88	73.43	68.20	50.31	52.05	49.90	123.74	464.51

Collection of strain data

The deformation and failure of bone is considered to follow a strain-controlled, ductile pattern [54]. Von Mises (VM) strain was therefore used to visually represent the magnitudes and distributions of deformation [37]. To examine deformation of the rostrum under each bite simulation, strain magnitudes were extracted from 13 locations in total from each model. These spanned the length of the cranium, however, unlike previous studies that collect strain data only from equidistant semilandmarks [43,54], we partitioned regions of the cranium using four fixed landmarks (landmarks 15, a midpoint between points 1 and 19, and 16 and 17 from the

GMM analyses) and added three equidistant semilandmarks between each successive pair (Fig. S4). This ensured that each landmark more accurately represented consistent regions of the crania across species with differing relative muzzle lengths. We used Landmark Editor (IDAV, Version 3.6) to allocate these. Average VM strain was calculated at each location from the bricks surrounding the focal node using custom code for Strand7, created by Samuel Evans, of the University of Newcastle.

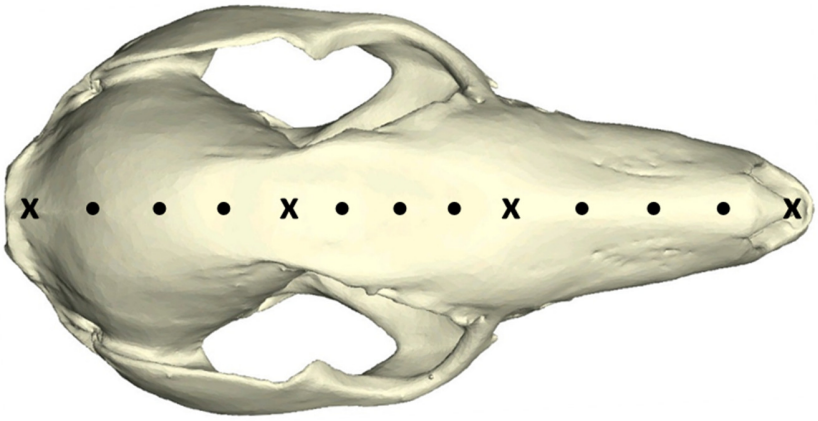

Figure S4: Landmarks (X) and semi-landmarks (•) for strain data collection.

REFERENCES

[1] Janis, C.M. 1990 Correlation of cranial and dental variables with body size in ungulates and macropodoids. In: Damuth, J. & MacFadden, B.J. (Eds). *Body size in mammalian paleobiology*, 255-299. Cambridge, Cambridge University Press.

[2] Milne, N. & O'Higgins, P. 2002 Inter-specific variation in *Macropus* crania: form, function and phylogeny. *J. Zool.* (Lond.) **256**, 523-535. (doi: 10.1017/S0952836902000572).

[3] Poole, W.E., Carpenter, S.M. & Simms, N.G. 1980 Multivariate analyses of skull morphometrics from the two species of grey kangaroos, *Macropus giganteus* Shaw and *M. fuliginosus* (Desmarest). *Aust. J. Zool.* **28**, 591-605.

[4] Kirkpatrick, T.H. 1964 Molar progression and macropod age. *Queensland J. Agric. Anim. Sci.* **21**, 163-165.

[5] Sanson, G. 1980 The morphology and occlusion of the molariform cheek teeth in some Macropodinae (Marsupialia: Macropodidae). *Aust. J. Zool*. **28**, 341-365.

[6] Sanson, G.D. 1989 Morphological adaptations of teeth to diets and feeding in the Macropodoidea. In: Grigg, G., Jarman, P. & Hume, I. (Eds.). *Kangaroos, Wallabies and Rat-kangaroos*, 151-168. NSW, Australia: Surrey Beatty.

[7] Arman, S.D. & Prideaux, G.J. 2015 Dietary classification of extant kangaroos and their relatives (Marsupialia: Macropodoidea). *Austral ecology* **40**, 909-922. (doi: 10.1111/aec.12273).

[8] Schlager, F.E. 1981 *The Distribution, Status and Ecology of the Rufous Rat-kangaroo, Aepyprymnus rufescens, in northern New South Wales*. Masters of Natural Resources, University of New England, Armidale.

[9] Seebeck, J.H.; Bennett, A.F. & Scotts, D.J. 1989 Ecology of Potoroidae - A review. In: Grigg, G., Jarman, P. & Hume, I. (Eds.*). Kangaroos, Wallabies and Rat-kangaroos*, 67-88. NSW, Australia: Surrey Beatty.

[10] Southwell, C. 1987 Macropod studies at Wallaby Creek. 2. Density and distribution of macropod species in relation to environmental variables. *Wildl. Res.* **14**, 15-33.

[11] Jarman, P.J. & Phillips, C.M. 1989 Diets in a community of macropod species. In: Grigg, G., Jarman, P. & Hume, I. (Eds.). *Kangaroos, Wallabies and Rat-kangaroos*, 143-149. NSW, Australia: Surrey Beatty.

[12] Wallis, I.R. 1990 *The nutrition, digestive physiology and metabolism of potoroine marsupials* (Doctoral dissertation, PhD thesis, University of New England, Armidale, Australia).

[13] McIlwee, A.P. & Johnson, C.N. 1998 The contribution of fungus to the diets of three mycophagous marsupials in Eucalyptus forests, revealed by stable isotope analysis. *Funct. Ecol.* **12**, 223-231. (doi: 10.1046/j.1365-2435.1998.00181.x).

[14] Dawson, T. J. 1989 Diets of macropodoid marsupials: general patterns and environmental influences. In: Grigg, G., Jarman, P. & Hume, I. (Eds.). *Kangaroos, Wallabies and Rat-kangaroos*, 129-142. NSW, Australia: Surrey Beatty.

[15] Dennis, A.J. 2002 The diet of the musky rat kangaroo, *Hypsiprymnodon moschatus*, a rainforest specialist. *Wildl. Res.* **29**, 209-219. (doi: 10.1071/WR00052).

[16] Lundie-Jenkins, G., Phillips, C.M. & Jaman, P.J. 1993 Ecology of the Rufous Hare-wallaby, *Lagorchestes hirsutus* Gould (Marsupialia : Macropodidae), in the Tanami Desert, Northern Territory. II. Diet and Feeding Strategy. *Wildl.* Res. **20**, 477-94

[17] Janis, C.M. 1990 Correlation of cranial and dental variables with dietary preferences in mammals: a comparison of macropodoids and ungulates. *Memoirs of the Queensland Museum* **28**, 349-366.

[18] Jarman, P.J. 1984 The dietary ecology of macropod marsupials. *Proceedings of the Nutrition Society of Australia* **9**, 82-87.

[19] Green, K., Davis, N.E., & Robinson, W.A. 2014 Does diet constrain the occupation of high elevations by macropods? A comparison between *Macropus rufogriseus* and *Wallabia bicolor*. *Austral. mammal.* **36**, 219-228. (doi: 10.1071/AM14007).

[20] Weir, A., McLeod, J., & Adams, C.E. 1995 The winter diet and parasitic fauna of a population of rednecked wallabies *Macropus rufogriseus* recently introduced to Scotland. *Mammal Review* **25**(3), 111-116.

[21] Green, K., Davis, N.E., & Robinson, W.A. 2015 The diet of the common wombat (*Vombatus ursinus*) above the winter snowline in the decade following a wildfire. *Austral. mammal.* **37**, 146-156. (doi: 10.1071/AM14037).

[22] Richardson, K. 2012 *Australia's Amazing Kangaroos: Their Conservation, Unique Biology and Coexistence with Humans.* CSIRO Publishing, Collingwood Victoria.

[23] Sprent, J.A. & McArthur, C. 2002 Diet and diet selection of two species in the macropodid browser–grazer continuum - do they eat what they should? *Aust. J. Zool*. **50**, 183-192. (doi: 10.1071/ZO01043).

[24] R Development Core Team. 2016 *R: a language and environment for statistical computing.* Vienna, Austria. URL http://www.R-project.org.

[25] Zelditch, M.L., Swiderski, D.L., Sheets, H.D. & Fink, W.L. 2004 *Geometric Morphometrics for Biologists: A Primer*. Elsevier, San Diego.

[26] Cardini, A., Polly, D., Dawson, R. & Milne, N. 2015 Why the long face? Kangaroos and wallabies follow the same 'rule' of cranial evolutionary allometry (CREA) as placentals. *Evol. Biol.* **42**, 169-176. (doi: 10.1007/s1169).

[27] Rohlf, F.J. & Slice, D. 1990 Extensions of the Procrustes Method for the Optimal Superimposition of Landmarks. *Syst. Zool.* **39**, 40-59.

[28] Adams, D.C., Collyer, M., Kaliontzopoulou, A. & Sherratt, E. 2016 Geomorph (Version 3.0.2,): Geometric Morphometric Analyses of 2D/3D Landmark Data.

[29] Klingenberg, C.P., Barluenga, M. & Meyer, A. 2002 Shape analysis of symmetric structures: quantifying variation among individuals and asymmetry. *Evolution* **56**, 1909-1920. (doi: 10.1554/0014-3820(2002)056[1909:SAOSSQ]2.0.CO;2).

[30] Adams, D.C. 2014 A method for assessing phylogenetic least squares models for shape and other high-dimensional multivariate data. *Evolution*, **68**, 2675-2688. (doi: 10.1111/evo.12463).

[31] Maddison, W.P. & Maddison, D.R. 2017 Mesquite: a modular system for evolutionary analysis. Version 3.31 http://mesquiteproject.org.

[32] Mitchell, K.J., Pratt, R.C., Watson, L.N., Gibb, G.C., Llamas, B., Kasper, M., Edson, J., Hopwood, B., Male, D., Armstrong, K.N., *et al.* 2014 Molecular Phylogeny, Biogeography, and Habitat Preference Evolution of Marsupials. *Mol. Biol. Evol.* **31**, 2322-2330. (doi: 10.1093/molbev/msu176).

[33] Phillips, M.J, Haouchar, D., Pratt, R.C., Gibb, G.C., Bunce, M. (2013) Inferring Kangaroo Phylogeny from Incongruent Nuclear and Mitochondrial Genes. *PLoS ONE* **8**, e57745. (doi: 10.1371/journal.pone.0057745).

[34] Klingenberg, C.P. 2013 Visualizations in geometric morphometrics: how to read and how to make graphs showing shape changes. *Hystrix* **24**, 15-14. (doi: 10.4404/hystrix-24.1-7691).

[35] Pinheiro, J., Bates, D., DebRoy, S., Sarkar, D. & Team, R. C. 2009 *nlme: Linear and nonlinear mixed effects models*. R package version, 3, 96.

[36] Wroe, S., Ferrara, T.L., McHenry, C.R., Curnoe, D. & Chamoli, U. 2010 The cranio-mandibular mechanics of being human. *Proc. R. Soc. Lond. **B** Biol. Sci.* **277**, 3579-3586. (doi: 10.1098/rspb.2010.0509).

[37] Ledogar, J.A., Luk, T.H.Y., Perry, J.M.G., Neaux, D. & Wroe, S. 2018 Biting mechanics and niche separation in a specialized clade of primate seed predators. *PLoS one*, **13**, e0190689. (doi: 10.1371/journal.pone.0190689).

[38] Dumont, E.R., Grosse, I.R., & Slater, G.J. 2009 Requirements for comparing the performance of finite element models of biological structures. *J. Theor. Biol*, **256**(1), 96-103. (doi: 10.1016/j.jtbi.2008.08.017).

[39] Strait, D.S., Grosse, I.R., Dechow, P.C., Smith, A.L., Wang, Q., Weber, G.W., Neubauer, S., Slice, D.E., Chalk, J., Richmond, B.G., *et al*. 2010 The structural rigidity of the cranium of *Australopithecus africanus*: implications for diet, dietary adaptations, and the allometry of feeding biomechanics. *Anat Rec*. **293**, 583-593. (doi: 10.1002/ar.21122).

[40] Walmsley, C.W., McCurry, M.R., Clausen, P.D. & McHenry, C.R. 2013 Beware the black box: investigating the sensitivity of FEA simulations to modelling factors in comparative biomechanics. *PeerJ* **1**, e204. (doi: 10.7717/peerj.204).

[41] Fitton, L.C., Prôa, M., Rowland, C., Toro-Ibacache, V. & O'higgins, P. 2015 The impact of simplifications on the performance of a finite element model of a *Macaca fascicularis* cranium. *Anat. Rec.* **298**, 107-121. (doi: 10.1002/ar.23075).

[42] Dumont, E.R., Piccirillo, J. & Grosse, I.R. 2005 Finite-element analysis of biting behavior and bone stress in the facial skeletons of bats. *Anat. Rec.* **283A**(2), 319-330. (doi: 10.1002/ar.a.20165).

[43] Sharp, A.C. 2015 Comparative finite element analysis of the cranial performance of four herbivorous marsupials. *J. Morphol.* **276**, 1230-1243. (doi: 10.1002/jmor.20414).

[44] Strait, D.S., Wang, Q., Dechow, P.C., Ross, C.F., Richmond, B.G., Spencer, M.A. & Patel, B.A. 2005 Modeling elastic properties in finite-element analysis: How much precision Is needed to produce an accurate model? *Anat. Rec*. **283A**, 275-287. (doi: 10.1002/ar.a.20172).

[45] Rayfield, E.J. 2007 Finite Element Analysis and Understanding the Biomechanics and Evolution of Living and Fossil Organisms. *Annu. Rev. Earth Planet. Sci.* **35**, 541-576. (doi: 10.1146/annurev.earth.35.031306.140104).

[46] Warburton, N.M. 2009 Comparative jaw muscle anatomy in kangaroos, wallabies, and rat-kangaroos (marsupialia: macropodoidea). *Anat. Rec*. **292**, 875-884. (doi: 10.1002/ar.20905).

[47] Strait, D.S., Wang, Q., Dechow, P.C., Ross, C.F., Richmond, B.G., Spencer, M.A. & Patel, B.A. 2005 Modeling elastic properties in finite-element analysis: How much precision is needed to produce an accurate model? *Anat. Rec. A Discov. Mol. Cell. Evol. Biol.* **283**, 275-287. (doi: 10.1002/ar.a.20172).

[48] Wroe, S., Chamoli, U., Parr, W.C., Clausen, P., Ridgely, R. & Witmer, L. 2013 Comparative biomechanical modeling of metatherian and placental saber-tooths: A different kind of bite for an extreme pouched predator. *PloS ONE* **8**, e66888. (doi: 10.1371/journal.pone.0066888).

[49] Grosse, I.R., Dumont, E.R., Coletta, C. & Tolleson, A. 2007 Techniques for modeling muscle-induced forces in finite element models of skeletal structures. *Anat. Rec.* **290**, 1069-1088. (doi: 10.1002/ar.20568).

[50] Myers, T.J. 2001 Prediction of marsupial body mass. *Aust. J. Zool*. **49**(2), 99-118. (doi: 10.1071/ZO01009).

[51] Wroe, S., McHenry, C. & Thomason, J. 2005 Bite club: comparative bite force in big biting mammals and the prediction of predatory behaviour in fossil taxa. *Proc. R. Soc. Lond., B, Biol. Sci.* **272**, 619-625. (doi: 10.1098/rspb.2004.2986).

[52] Greaves, W. S. 1978 The jaw lever system in ungulates: a new model. *J. Zool.*, **184**(2), 271-285.

[53] McHenry, C.R., Wroe, S., Clausen, P.D., Moreno, K. & Cunningham, E. 2007 Supermodeled sabercat, predatory behavior in *Smilodon fatalis* revealed by high-resolution 3D computer simulation. *Proc. Natl. Acad. Sci. U.S.A.* **104**, 16010-16015. (doi: 10.1073/pnas.0706086104).

[54] Nalla, R.K., Kinney, J.H. & Ritchie, R.O. 2003 Mechanistic fracture criteria for the failure of human cortical bone. *Nat. Mater.* **2**, 164–168. (doi: 10.1038/nmat832).

[55] Attard, M.R., Parr, W.C., Wilson, L.A., Archer, M., Hand, S.J., Rogers, T.L. & Wroe, S. 2014. Virtual reconstruction and prey size preference in the mid Cenozoic thylacinid, *Nimbacinus dicksoni* (Thylacinidae, Marsupialia). *PloS one*, **9**(4), e93088. (doi: 10.1111/j.1469-7998.2011.00844.x).